Reshaping End-of-Life components by sheet hydroforming: an experimental and numerical analysis

A. Piccininni[1], A. Cusanno[1], G. Palumbo[1], O. Zaheer[2], G. Ingarao[2], L. Fratini[2]

[1]Dept. of Mechanics, Mathematics and Management, Politecnico di Bari, Via Orabona 4, 70125 Bari

[2] Department of Engineering, University of Palermo, Viale delle Scienze, Palermo, 90128, Italy

ABSTRACT

In this study, a numerical/experimental analysis is proposed to investigate the possibility of reshaping sheet metal-based End-of-Life (EoL) components using sheet Hydroforming (SHF). Returned EoL components are challenging to be reformed, they are usually characterised by high heterogeneity as there are localised thinning areas (caused by the original forming processes), and the overall formability is reduced with respect to the original flat sheet material. The reshaping route was replicated: a deep drawing process was adopted to impart a square feature; subsequently, SHF was performed. The capability of remove the deep drawn feature was analysed with varying Blank-holder force, oil pressure profile and the location of the previous deep drawn feature. A 3D finite element model of the entire manufacturing route was used to analyse the strain paths of the reshaping process. The change in the strain paths when considering a component previously subjected to deep drawing was analysed and discussed in comparison with SHF using an undeformed blank. This study for the first time provides an insight on the reshaping process mechanics as well as attempts at quantifying the quality of the reshaped components. Results revealed that SHF can be successfully adopted for reshaping purposes as it performed well under two analysed aspects: capability of removing the existing feature and imparting a brand-new shape and thickness/strain path analyses (avoiding fracture and excessive thinning). Nevertheless, the developed analyses revealed that reshaping is more challenging than conventional forming and new design rules, identified in the present paper, need to be followed.

Keywords: Reshaping, Sheet Hydroforming, Al alloy, FEM

1. INTRODUCTION

Currently, lowering the anthropogenic environmental impact is a pressing need. In this respect, materials production plays a significant role: the conversion of resources extracted from natural ecosystems into usable materials results in considerable energy consumption and carbon dioxide (CO_2) emissions. Only five key materials (aluminium, steel, cement, paper, and plastic) account for approximately half of all annual greenhouse gas (GHG) emissions released by industries worldwide (Sutherland et al., 2020). The primary production of materials is energy and emission intensive, with aluminium production being the most emission intensive among the aforementioned key materials (Worrell et al., 2016). Aluminium alloys production alone accounts for almost 1% of the total worldwide GHG emissions annually (Milovanoff et al., 2021). Moreover, since 1971, the global demand for steel has increased by three times, cement by nearly seven times, primary aluminium by nearly six times, and plastics by more than ten times (IEA, 2019). The demand for raw materials

has been reduced to reduce both anthropogenic CO_2 emissions and decouple economic growth from resource consumption. Strategies that entail the use of less materials and keeping as much material as possible in the circle are becoming increasingly mandatory.

The circular economy (CE) is a well-recognised paradigm based on several strategies to reduce the environmental impact of raw material production (Tolio et al., 2017). The basic idea is to turn end-of-life (EoL) products/components directly into reusable materials or, better yet, into new products/components. Although recycling is the most commonly applied strategy when metals are concerned, there is still room for improvement in the energy and resource efficiency. In the case of aluminium alloys, the functional recovery allows further energy savings(Zhang et al., 2020): literature reports a framework for metal reuse, in which four main strategies – relocation, cascade, remanufacturing, and reform/reshaping – are identified (Cooper and Allwood, 2012). The firsts two envisage a superficial reconditioning and neither advanced manufacturing skills nor processes are required. In contrast, remanufacturing and reform/reshaping are characterised by extensive reconditioning, and manufacturing processes are extensively employed for enabling such circular economy strategies. In the reshape/reform context, manufacturing processes become even more significant as they are applied directly to the EoL component to obtain a new, more useful geometry. Therefore, manufacturing scientists are called to rethink and/or find new manufacturing processes suitable for EoL metal components remanufacturing and reshaping.

Although remanufacturing has been extensively analysed by manufacturing scientists over the last few years (Tolio et al., 2017), the reshaping strategy has been overlooked by the scientific community to date. In general, most research is concerned with additive manufacturing applications, often coupled with machining processes, either to repair or to change the EoL geometry (Le et al., 2018). On the contrary, forming processes applied as a reshaping strategy have been mentioned in very few scientific publications: for instance, Tilwankar et al. (Tilwankar et al., 2008) proposed to reroll steel recovered from vessels into semi-finished products (plates, bars, and rods used). But it should be remarked that sheets (including strips and foil production) account for approximately 40% of the annual global aluminium alloys demand (Cullen and Allwood, 2013). Thus, the possibility to produce a component starting from a part already subjected to a previous sheet forming process is largely attractive, even from the social and economic point of view. Some authors of the present paper have recently investigated the use of Single Point Incremental Forming (SPIF) to change the shape of a previously deep drawn square box, demonstrating the lower energy consumption with respect to a conventional recycling strategy (Ingarao et al., 2021).

Sheet metal forming processes which can be considered as "flexible" (for example: incremental forming, hydroforming, gas forming) are ideal candidates for reshaping (Jeswiet et al., 2008). For example, Takano et al. (Takano et al., 2008) applied single-point incremental forming (SPIF) to reform a previously bent sheet, where flattening of the EoL component was envisaged prior to the incremental forming application; Abu-Farha and Khraisheh (Abu-Farha and Khraisheh, 2008) proposed the application of superplastic forming to reshape EoL magnesium sheet components; Brosius et al. (Brosius et al., 2009) included a description in a review paper of how a demounted automotive engine hood can be reshaped into a rectangular sheet metal component by

Sheet HydroForming (SHF). Such a process has several advantages over other forming processes (Bell et al., 2020), such as: (i) enhanced formability limits (Lang et al., 2004); (ii) more complex shapes including the creation of re-entrant features (Parsa and Darbandi, 2008) and/or a lower number of forming steps (Sato et al., 2015); and (iii) reduced thinning and better thickness distribution.

It should be also considered that the reshaping approach is yet to be fully understood, and the most suitable forming processes for reshaping purposes must be identified: there is a lack of process mechanics analyses, and neither process windows nor the influence of process parameters has been sufficiently analysed so far. It is also important to highlight that EoL components are usually characterised by high heterogeneity, as thinning could be located in some specific areas (caused by the first manufacturing processes), while the remaining part of the component experienced limited deformation. Thus, formability conditions might change significantly across the components: the thinned zones may be characterised by a limited residual formability, while in the less formed zones, the original formability of the virgin (flat sheet) material is likely to retain. Along with formability/stampability issues other challenges need to be taken into account when dealing with Reshaping. EoL product recovery, sheet part disassembly, inspection, de-coating and reshaping are all the steps required to put in place such an approach at industrial scale. Specifically, inspection for thinning distribution is fundamental for designing the subsequent reshaping operations. Also, de-coating could affect the reshaping process (these processes normally take place at elevated temperatures) and the effect of the sheet heating on the mechanical properties should be taken into account properly. These aspects together with changes in thickness or properties during the usage (although detected during the inspection steps) could make this approach even more challenging. The present paper deals with the manufacturing process related challenge: identifying the correct processes for reshaping able to convert a given sheet metal EoL shape into a brand new one. The reshaping process must be capable to deal with a kind of undesired pre-deformation step, in particular it must be capable to remove any existing feature while providing a new shape.

In this paper, the SHF process is proposed as reshaping route, providing for the first time an insight on the process mechanics and attempting at quantifying the quality of the reshaped components. A deep drawn part was chosen as a possible EoL component, being the Deep Drawing process one of the most common sheet metal forming process used for industrial applications; in addition, it determines a non-homogeneous strain distribution. Thus, the Reshaping route based on a deep-drawn EoL component subsequently deformed by hydroforming has been assumed as case study, being close enough to the real situation in which the proposed approach could be adopted. The present study aims at covering the highlighted gap of knowledge in the application of the reshaping as a valid and more sustainable production approach, especially for aluminium sheet metal-based EoL components.

2. Material and methods

The authors converted a virgin blank into an EoL component by imparting deformations to achieve the research objectives. Deep drawing (DD) was performed on a virgin blank, where it was considered as the first manufacturing process to resemble an EoL component. The EoL component obtained after deep drawing was

reshaped by performing an SHF process on the component. The feasibility of this reshaping strategy was investigated by analysing the effects of variations in the SHF process parameters as well as the positioning of the deep drawn feature. Figure 1 shows a graphical synthesis of the proposed method. The experimental campaign consisted of two steps: DD followed by SHF of AA5754 H22 aluminium alloy sheets (thickness: 0.5 mm).
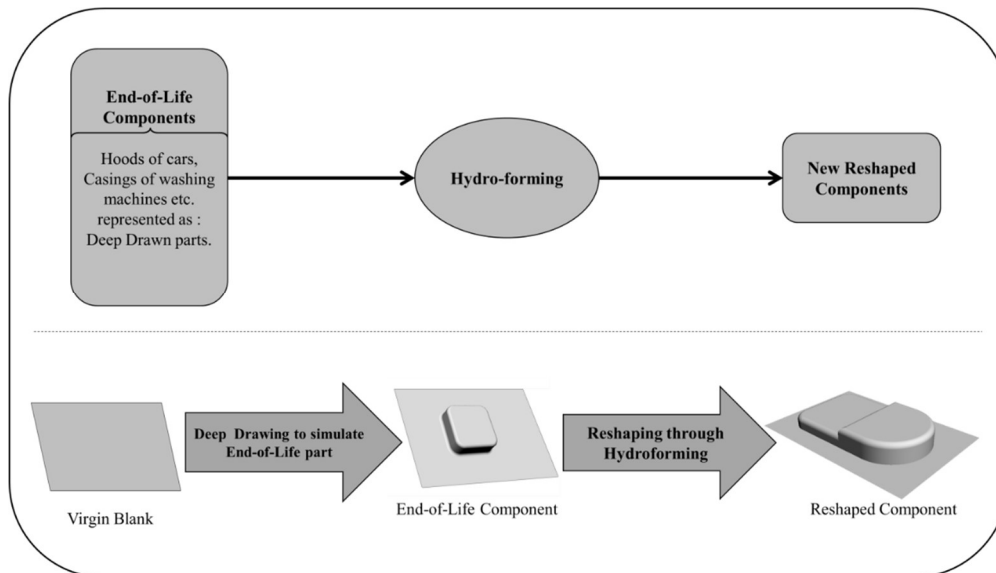

Figure 1 Overview of the proposed methodology

It is worth remarking that the choice of the Deep Drawing process to obtain the EoL component was selected as a proxy of a worst-case scenario. The selected Deep Drawn feature is characterised by localised thinning and strains phenomena as well as by high rigidity, thus it is a very challenging feature to be removed and converted into a brand-new shape. On the contrary, a big share of large panels of EoL components are characterised by lower and more homogenous deformation levels. Actually, slight and homogenous curvature or simple features for providing rigidity or functionalities are normally imparted in many sheets metal components.

2.1 Experimental setup for Deep Drawing

The DD process was performed using a Galdabini Quasar 600 hydraulic press. The tools utilised comprised a die, punch, and a blank holder. The DD process was performed on rectangular blanks with a blank holder force (BHF) increasing linearly from 2027 N to 4202 N and a constant punch velocity of 1 mm/s. Figure 2 illustrates the system used for the DD process (a) and the geometric parameters of the resulting component (b).
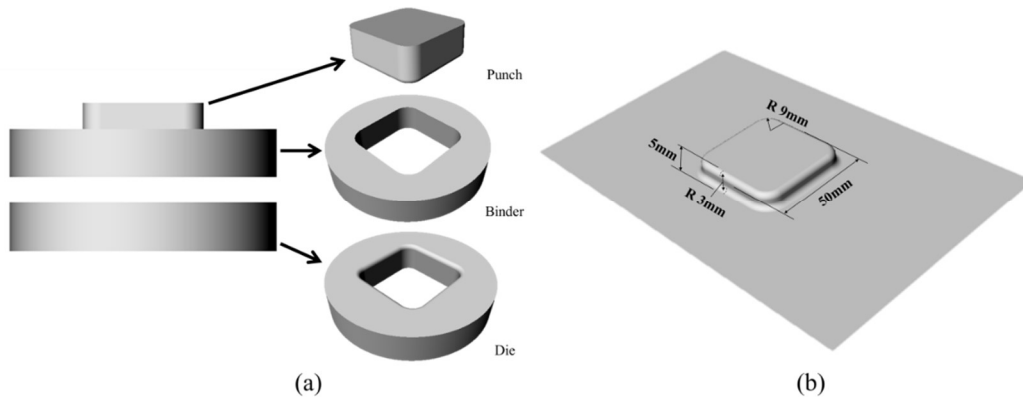
Figure 2 (a) Deep drawing system; (b) Geometrical features of the deep drawn component

The selected EoL component is characterised by localized strain levels located at the bottom corner of the Deep Drawn feature (see Figure 12). On the contrary, in the flange and at the base of the feature very low (almost zero in the flange) strain levels occur. The selected part, therefore, is successful in mimicking an EoL component in terms of heterogeneity of the strain hardening and the thickness distribution.

2.2 SHF experimental tests

SHF test were carried out using a 2500 kN (4 electric motors supported by additional 2 hydraulic cylinders for increasing the closing force) prototype electro-hydraulic press machine (Palumbo et al., 2015). The press is equipped with heated tool to carry out the hydroforming process also in warm conditions, up to a temperature of 350°C. As shown in Figure 3a, hydroforming tools are composed of a die (upper tool) and a blank-holder (lower tool) that, during forming operation in warm conditions, are both heated by Nickel Alloy 600 plates embedding electric cartridges (total power: 24 kW). Moreover, two refractory plates and a lateral insulating wall limit the heat dispersion during the process. Heating elements embedded in both tools are managed by a programmable logic controller (PLC), so that temperature can be regulated using the acquisition from thermocouples placed in proximity of the surfaces of the die and of the blank holder. The geometry of the die, whose main dimensions are reported in Figure 3b, is characterised by a two-step cavity (depths of 12 mm and 20 mm, respectively).
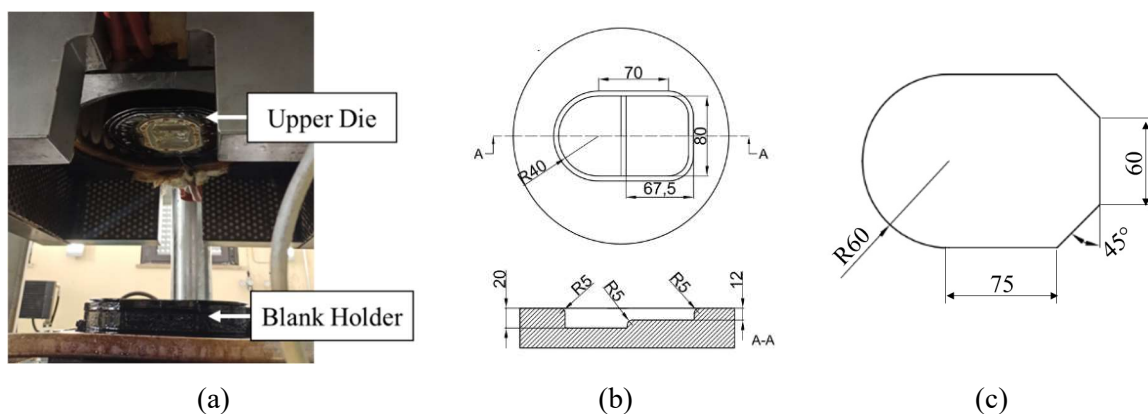
Figure 3 (a) Equipment used for the experimental SHF tests; (b) Geometrical features of the case study; (c) Optimised initial blank geometry

For the present research all the tests were carried out at room temperature. Prior to performing the SHF test, the deep drawn blanks were cut to modify the external profile according to the geometry shown in Figure 3c. Such an external profile was designed using numerical simulations to optimise the material drawing. Different operating conditions were investigated based on the location of the DD feature on a flat blank.

- *TOP* (Figure *4*a): The DD feature is located close to the circular part of the blank profile, and consequently, it is in front of the deepest (20 mm) region of the die cavity during the SHF process.
- *BOTTOM* (Figure *4*b): The DD feature is located opposite to the circular part of the blank profile and, consequently, is in front of the shallowest (12 mm) region of the die cavity during the SHF process.
- *MIDDLE* (Figure *4*c): The DD feature is located in the middle of the initial blank and, consequently, the feature is placed between the two cavities during the SHF process.
- *Only SHF* (Figure *4*d): there is no DD feature on the blank, which was subjected to SHF; this condition was used for comparison purposes.

| (a) | (b) | (c) | (d) |
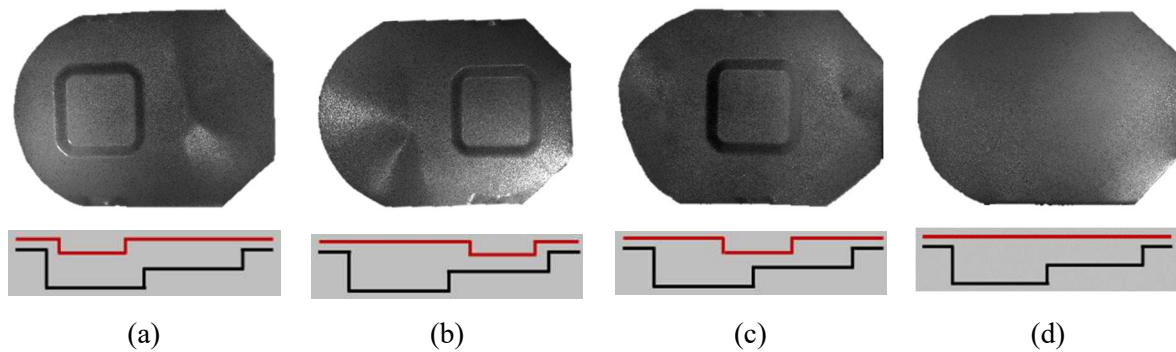
Figure 4 (a) TOP, (b) BOTTOM (c) MIDDLE and (d) Only SHF conditions in the case of SHF tests; the red line indicates the starting blank for SHF tests; the black line represents the die cavity.

At the end of the DD step, the blank was placed in the SHF setup and subjected to the reshaping process. The parameters controlled during tests were the Blank-Holder Force (BHF) and the oil pressure. The latter was controlled by a proportional electronic valve (maximum pressure: 350 bar) managed by the PLC which allowed to increase the oil pressure according to the linear profile reported in Figure 5 (the oil pressure able to deform the material was increased only when the BHF reached the target initial value BHF_{in}).
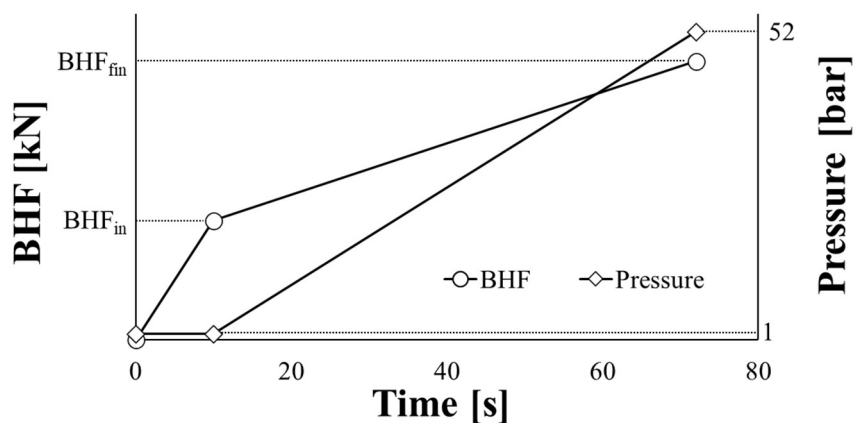
Figure 5 BHF and pressure profiles adopted during the SHF step

Such an oil pressure profile was kept unchanged for all tests, linearly increasing from 1 bar to 52 bar (rate: 1 bar/s). Even though literature reports examples of optimized BHF profiles (Cao and Boyce, 1997), SHF tests as reshaping attempts were conducted changing both the initial (BHF_{in}) and the final BHF (BHF_{fin}) values being more focused on the formability-related issues; in particular, two levels for both BHF_{in} (13 kN – 33 kN) and BHF_{fin} (57 kN – 77 kN) were adopted, being such values able to combine the need to maximize the die cavity filling and to avoid premature fractures. The location of the deep drawn feature was also investigated: three different locations of the deep drawn feature (TOP, MIDDLE, BOTTOM) were investigated. Finally, the condition "Only SHF" was also investigated for comparison purposes.

2.3 Geometrical Acquisition Setup

After performing the two forming processes, the resulting components were scanned using the 3DPhoto Acquisition system 'Steinbichler Comet' to obtain 3D models for analysis. The used 3D scanner is based on structured light technique using fringe projection with an accuracy equal to 0.015 mm. The output of the scanning process is the STL file of acquired geometry that is further processed for analysing the shape accuracy of the reshaped components: geometric deviations occurring in the reshaped components were quantified by comparing the obtained geometry to that obtained by performing SHF using flat blanks (while maintaining the process parameters unchanged). The comparison was performed using 3D quality control and dimensional inspection software, 'Geomagic Control X'. Within Geomagic Control X environment it is possible to optimize the alignment of two surfaces by the application of the iterative closest point algorithm which minimises the sums of squares of distances between the sample pairs. Accordingly, the maximum deviation and standard deviation were recorded as metrics for the quantification of the geometric accuracy, and the results are discussed in Section 3.

2.4 FE Model

The entire reshaping process chain, that is the preliminary DD step and subsequent SHF step, was simulated using the FE commercial code Abaqus. The strain distribution and its evolution throughout the whole processing route, as well as the final thickness distribution, could be investigated and correctly predicted using the FE model. In such a way it will be possible to design the reshaping process (i.e, to define the process parameters able to remove the previous shape of the component).

An explicit solver was employed to simulate both steps. To reduce the computation time, only half of the system was modelled (see Figure 6) and a semi-automatic mass scaling approach was adopted (among different tested values of the stable time increment, the largest one able to the keep the system's kinetic energy negligible with respect to the internal energy was chosen).
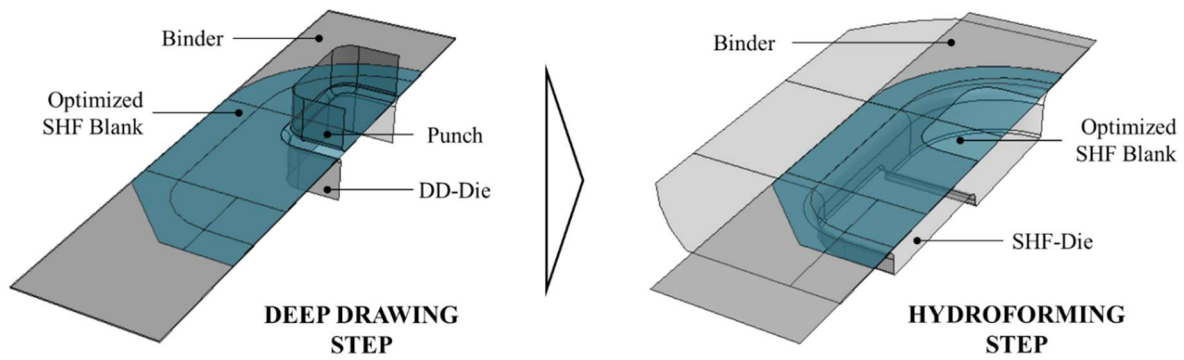
Figure 6 FE simulation of the reshaping process

Material data were implemented in the FE model in terms of flow stress curve (from tensile test carried out on dog-bone specimen according to the UNI EN ISO 6892) and the forming limit curve (Ingarao et al., 2020). The latter made it possible to activate an FLC-based damage criterion that could provide information regarding the strain severity over the reshaped blank.

Regardless of the specific manufacturing step, the tools were modelled as discrete 3D shell rigid bodies, whereas the blank was modelled as a 3D shell deformable body setting for the section properties the initial thickness to 0.5 mm and the integration points to 5. The rigid surfaces were meshed using R3D3 and R3D4 elements (3 and 4 nodes rigid element) with a coarser element size; considering the dimensions reported in Figure 3, the size of 5mm was considered fine enough to correctly discretize the region of the die entry radius and the one of the fillet radius between the two steps. On the contrary, the blank was discretised using S4R and S3R shell elements; since the mesh size largely affects the computing time, the value was set to 1 mm according to the need of getting accurate enough results and limiting the computing time. The interactions between rigid and deformable bodies were modelled using the 'surface-to-surface' contact discretisation algorithm. The friction was modelled using the Coulomb's formulation and setting the coefficient to 0.125 (Domitner et al., 2021). The two manufacturing steps (i.e., the preliminary DD followed by SHF), were sequentially simulated using the same FE model. Since the tools for both steps were modelled within the same assembly, the relative contact pairs with the blank were sequentially activated (or deactivated) according to the step under investigation. In both manufacturing steps, the blank was modelled using the shape shown in Figure 6.
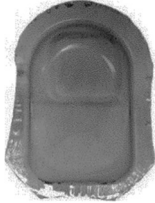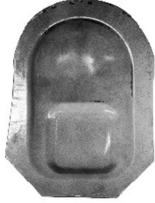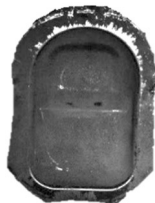
3. Results and Discussion

3.1 Experimental results

Table 1 presents an overview of the experimental results obtained after the SHF step. For each condition, the values of the input parameters (BHF_{in} and BHF_{fin}) and the initial position of the feature are specified, and the final shape obtained is shown. It can be seen whether the final part is safe (absence of ductile fracture) or not. Some combinations of process parameters did not allow sound parts to be obtained, and ductile fracture occurred close to the central fillet radius. As concerns fractures, they were observed for the highest values of

BHF (ID 10,11,12) and, as expected, a higher level of restraining forces resulted in excessive stretching mechanics, leading to fracture conditions. All the investigated operating conditions were replicated three times and a high level of accordance among replications was achieved.

Table 1 Results of the experimental plan for the SHF test

ID	ID01	ID02	ID03	ID04
BHF$_{in}$ [kN]	13	13	13	13
BHF$_{fin}$ [kN]	57	57	57	77
Position of the feature	TOP	MIDDLE	BOTTOM	TOP
Safe	Yes	Yes	Yes	Yes

ID	ID05	ID06	ID07	ID08
BHF$_{in}$ [kN]	13	13	33	33
BHF$_{fin}$ [kN]	77	77	57	57
Position of the feature	MIDDLE	BOTTOM	TOP	MIDDLE
Safe	Yes	Yes	Yes	Yes

ID	ID09	ID10	ID11	ID12
BHF$_{in}$ [kN]	33	33	33	33
BHF$_{fin}$ [kN]	57	77	77	77
Position of the feature	BOTTOM	TOP	MIDDLE	BOTTOM
Safe	YES	NO	NO	NO

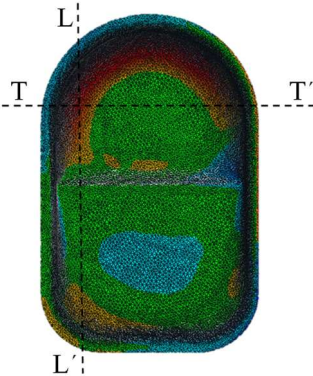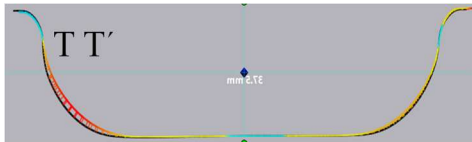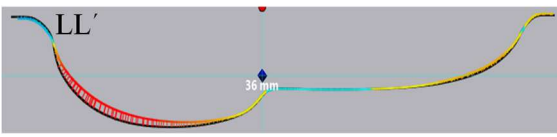| ID	ID13	ID14	ID15	ID16
BHF$_{in}$ [kN]	33	13	13	33
BHF$_{fin}$ [kN]	57	77	57	77
Position of the feature	Only SHF	Only SHF	Only SHF	Only SHF
Safe	Yes	Yes	Yes	Yes

3.1.1 Geometric accuracy analysis

Two different analyses were developed to evaluate the geometric accuracy: global and local analyses. A global analysis was performed on the entire surface, whereas a local analysis was developed on a narrowed area to better quantify the presence of the DD feature in the reshaped component.
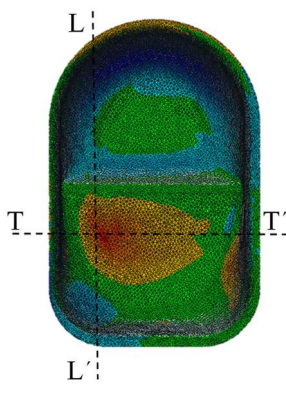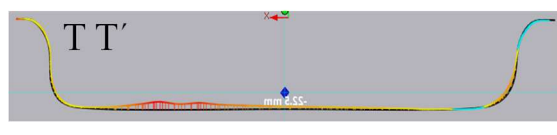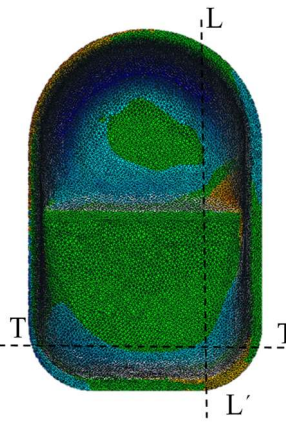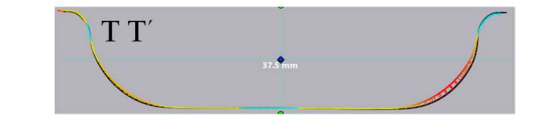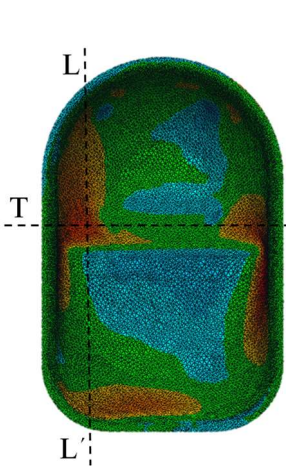
For the global analysis, for each ID, the final reshaped surface was compared with the corresponding parts obtained on the SHF of a virgin blank with the same parameters. Since only sound parts were considered for the geometrical analyses, IDs 10, 11, and 12 were excluded from the subsequent statistical analyses.
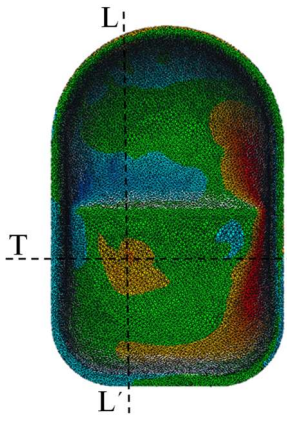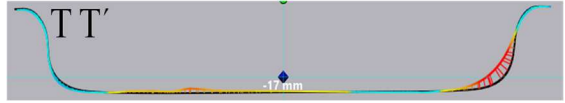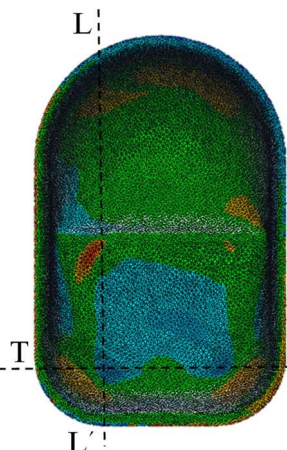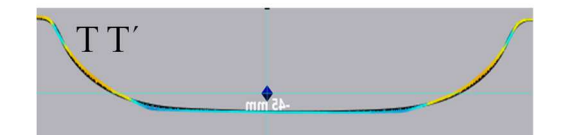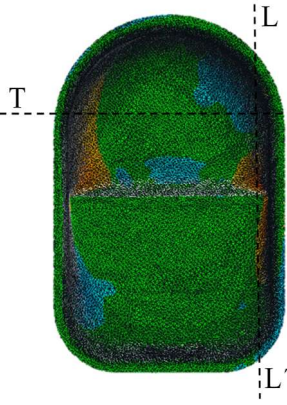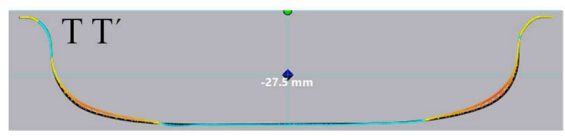
For each ID, the maximum deviation and standard deviation values were recorded as metrics to quantify geometrical accuracy. The results are reported in Table 2, where the error maps are reported along with the analyses of significant section views (i.e. where the maximum deviations were observed): each operating condition, beside the progressive ID, is uniquely identified by a code composed of a capitol letter describing the position of the deep-drawn feature (T for TOP, M for MIDDLE and B for BOTTOM) followed by the initial and final values of the BHF (expressed in kN).
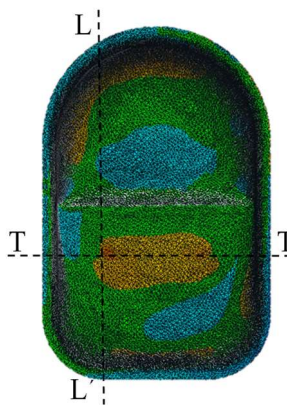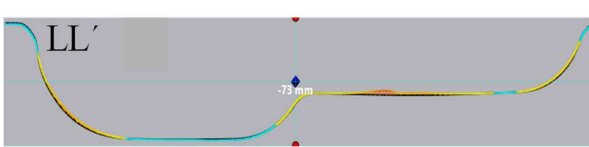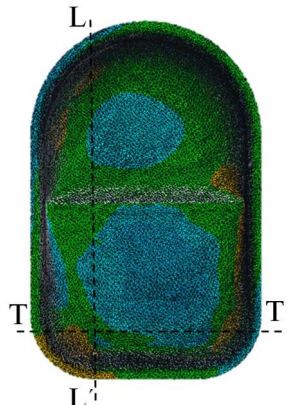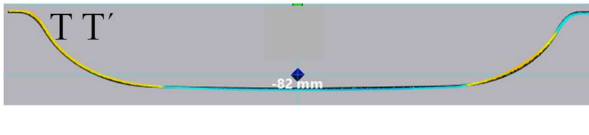
Both dark red and dark blue colours in the map correspond to high maximum deviation values: blue zones correspond to negative deviations, whereas red zones correspond to positive deviations with respect to the reference geometry (black contour in the Section View of Table 2), and the absolute values of the deviation are reported for the sake of clarity.

Table 2 Results of the geometric accuracy analysis for the reshaping by SHF tests

ID	Geometric Analysis	Section View	Maximum Dev [mm]	Std. Dev [mm]
ID 01 T_13-57			1.52	0.39

ID 02 **M_13-57**		T T′ LL′	1.13	0.35
ID 03 **B_13-57**		T T′ LL′	1.40	0.39
ID 04 **T_13-77**		T T′ LL′	1.17	0.23

ID 05 M_13-77			1.75	0.33
ID 06 B_13-77			1.59	0.24
ID 07 T_33-57			0.92	0.16
ID 08 M_33-57			0.70	0.17

				0.63	0.15

ID 09 B_33-57

Evidently, it can be stated that the difference in terms of the final shape is limited, as the starting blanks (virgin/flat vs. deep drawn) are characterised by different hardening levels, and the material flow during SHF is different, although the same process parameters were used.

Main effect plot analyses were carried out to gain a clearer overview of the influence of the process parameters on the global geometric inaccuracies, and the results are presented in Figure 7 in terms of the maximum deviation (MAX DEV) and standard deviation (STD DEV).

Figure 7 Main effects plots for the maximum and standard deviations recorded from the geometrical accuracy analysis of the reshaped components

It can be observed that when the BHF values increase, the shape accuracy improves. It can be attributed to the change in process mechanics caused by the increase of the restraining forces: the increase of the BHF enables larger stretching mechanics in the sheet while it is hydroformed. Such a phenomen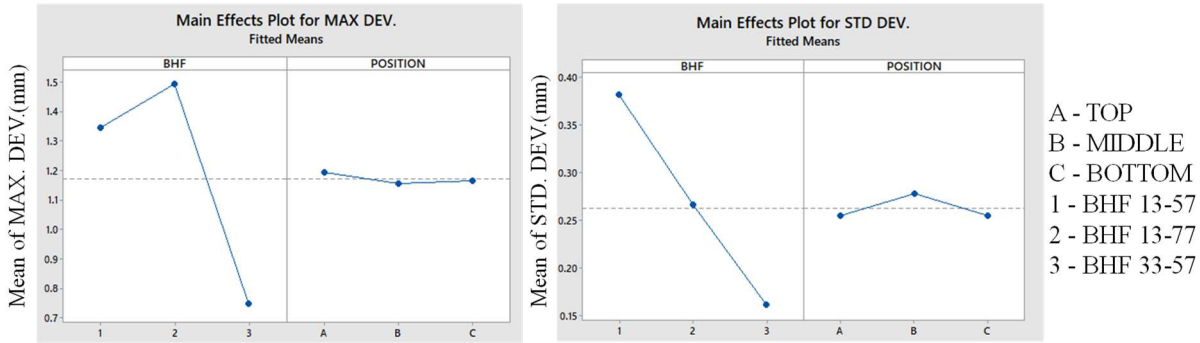on definitely helps in removing the deep drawn feature and to reduce the geometrical difference with respect to the component obtained only by SHF.

A local analysis was also developed to better quantify the extent to which the feature was still present in the hydroformed component. The bottom corners proved to be the most difficult regions of the DD feature to be removed by reshaping. Consequently, the local analysis was narrowed on such regions, and the maximum deviation in this zone was quantified for each ID. The recorded maximum deviation values are reported in Figure 8.
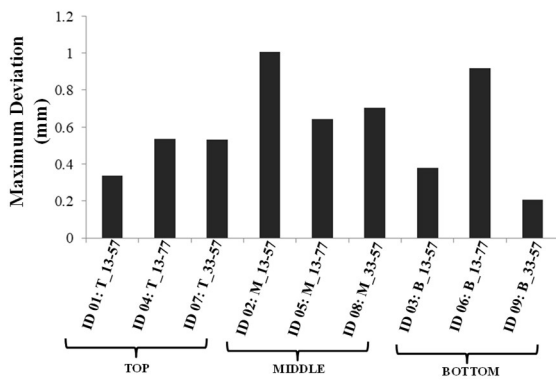
Figure 8 Maximum deviation values recorded on the local analysis of the components.
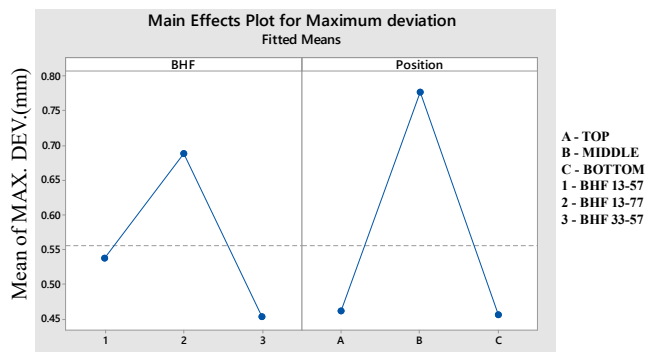
Figure 9 Main effects plots for the maximum deviation values recorded on the local analysis of the components.

The results reported in Figure 8 does not provide a clear trend regarding the impact of the feature position and of the BHF level on the local geometrical analysis. For the sake of clarity, the main effect plot was developed, and results are reported in Figure 9. It can be observed that the largest beneficial impact of the BHF is related to its initial value, which probably affects more the material drawing in combination with the position of the previous feature, thus limiting the geometrical error. The main effect plot also reveals that MIDDLE position of the feature has a significant impact since it probably affects the EoL stiffness and, at the same time, the level of the strain which the material can still experience. This result can be explained considering that, when the feature is located in MIDDLE position, the edge of the deep drawn feature undergoes a bending action when the blank gets in contact with the fillet radius between the two steps. The edge of the deep drawn feature is a rigid and hardened area, therefore part of the provided deformation energy is committed in such bending rather than in the feature removal. Such phenomenon does not occur when the feature is located in TOP and BOTTOM region.

In Figure 10 the attention is focused on the samples which showed the highest (ID02 - MIDDLE) and lowest (ID09 - BOTTOM) maximum deviation values by showing a local fitting analysis (in the most deformed region from the preliminary DD step) and two section cut views. It can be noted that the deep drawn feature was still visible in ID02, while almost no shape defect could be observed in ID09.
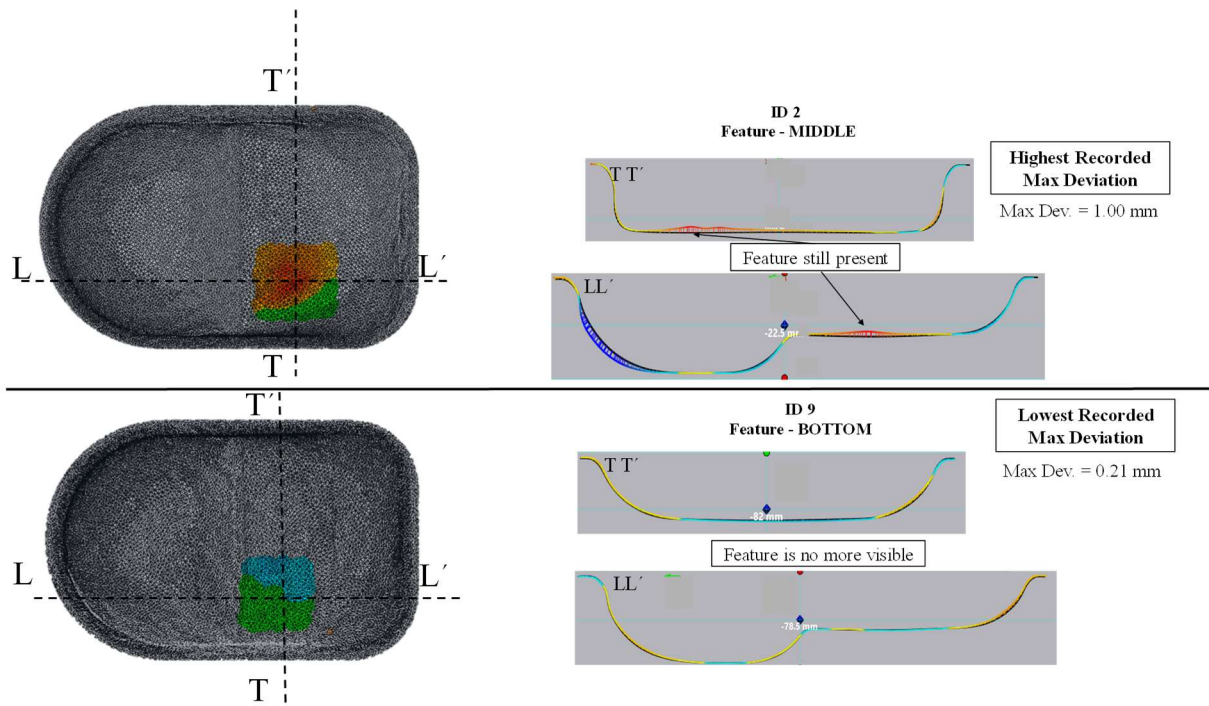
Figure 10 Local analysis and section cut view of ID02 and ID09.

This result is confirmed by the visual inspection of the two mentioned specimens. As shown in Figure 11, ID02 exhibited evident marks, particularly in the corner regions, owing to the preliminary DD step.
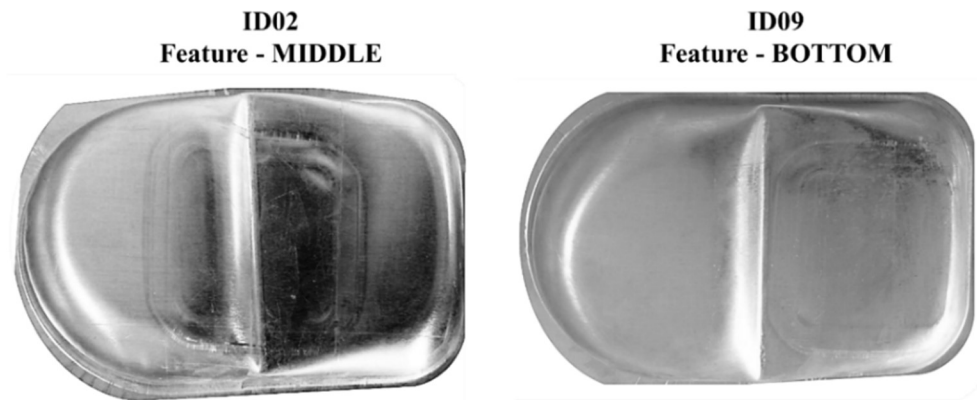
Figure 11 Visual appearance of the ID02 and ID09 at the end of the reshaping by SHF

However, even though reshaping by SHF imparted smaller strains to the portion of the blank in contact with the shallow step, the marks on ID09 were far less evident. Nevertheless, the overall results revealed that the feature is more visible in the bottom region; this can be clearly deduced by looking in Table 2 in which it can be seen that the maximum deviation always occurred for the tests labelled as MIDDLE (ID02, ID05, ID08) and that the error assumed the maximum values in the bottom region. Consequently, the smaller the strain level that occurs during the reshaping step, the more difficult it is to remove the previous feature, thus confirming the motivation of the bad performance shown in Figure 8 and Figure 9 when considering the MIDDLE position.

3.2 Numerical Results

The reshaping process was simulated by modelling the blank with the same initial shape (the one used for the SHF), which represented a slight difference from the experimental procedure in which the DD was performed on a rectangular blank. Nevertheless, the small amount of strain reached in the neighbouring region of the deep drawn feature justifies this assumption.

The numerical results at the end of the reshaping step were analysed in terms of the plastic equivalent strain (PEEQ) and FLDCRT (which is an output that quantifies how far the nodal strain condition is from the FLC). For example, the final distributions of the two variables regarding the operative condition of ID04 (T_13-77) are shown in Figure 12.
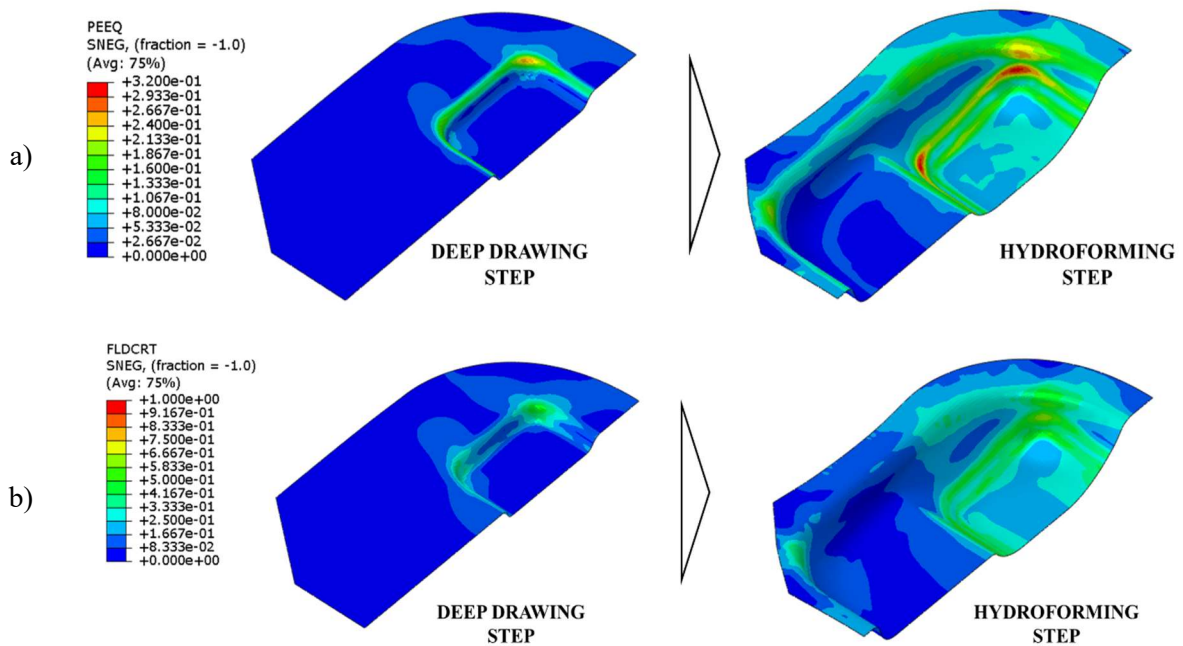
Figure 12 Numerical results concerning the test ID04 (T_13-77): a) PEEQ and b) FLDCRT nodal distributions

As expected, at the end of the DD step, the corner region was characterised by the largest strain, which was also confirmed by the higher values of FLDCRT. Moreover, the PEEQ distribution in Figure 12a indicates that these regions remained more strained even at the end of the SHF step when compared to the other regions of the blank, characterised by a lower level of equivalent plastic strain. Similar considerations can be drawn by observing the FLDCRT distribution map in Figure 12b: even though the implementation of the FLC could only provide some qualitative information (owing to the change in the nodal strain path during the reshaping), the region previously deformed by DD maintained a more severe strain condition.

3.2.1 Experimental validation of the numerical results

In this study, the accuracy of the numerical methodology was assessed by focusing the attention on the test ID08 (M_33-57). The experimental acquisitions were compared to the numerical predictions in terms of both 2D deformed profile and final thickness distributions. As concerns the former, Figure 13a shows the limited discrepancy between the numerical and experimental 2D profiles extracted using the longitudinal symmetry

plane: the maximum deviation was equal to 1.17 mm (located in the blank region in contact with the deepest part of the die). The accuracy of the FE model was further confirmed by the comparison of the thickness profiles along the same longitudinal direction (indicated by the red line in Figure 13): the difference between the numerical and experimental thickness values was always lower than 0.02 mm (approximately 4% of the undeformed blank thickness).

a)

b)
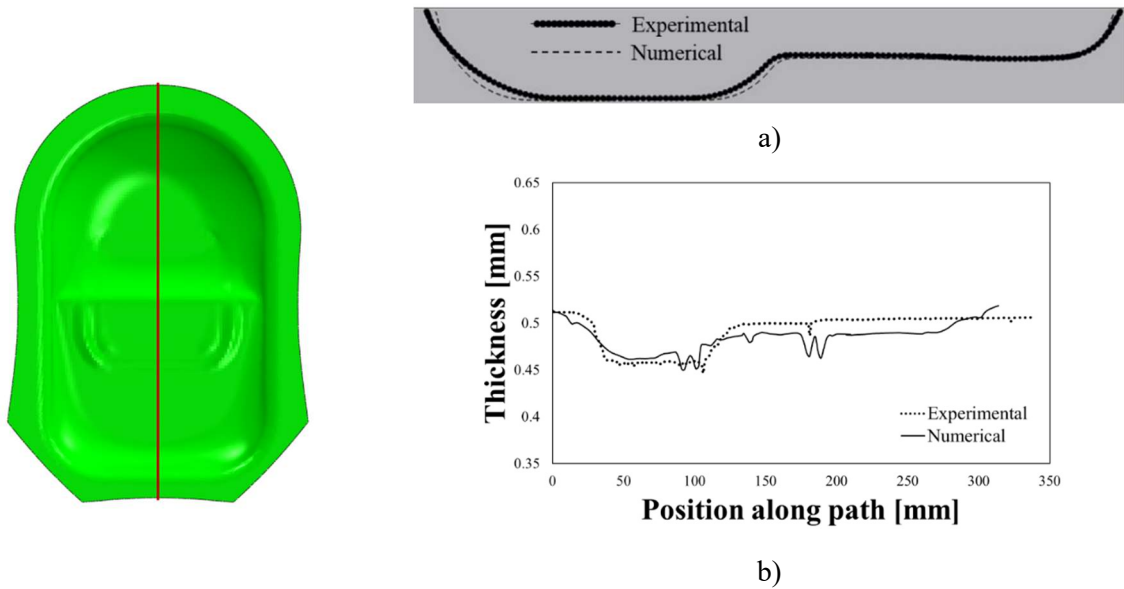
Figure 13 Experimental validation of the numerical results (ID08): (a) deformed shape and (b) thickness distribution (ID08)

The numerical results allowed to highlight the local thinning due to the presence of the deep drawn feature, giving a more precise description of the thickness distribution than what the experimental method could provide. The adopted FE model also gave the additional advantage of evaluating to what extend the SHF step was able to remove the preliminary DD step. To better support this consideration, the deformed shapes from the numerical simulation were compared to the correspondent experimental ones considering the three possible locations of the deep drawn feature. The comparison proposed in Figure 14 demonstrates the very good fitting for three IDs characterised by a different location of the deep drawn feature.

a)   b)   c)
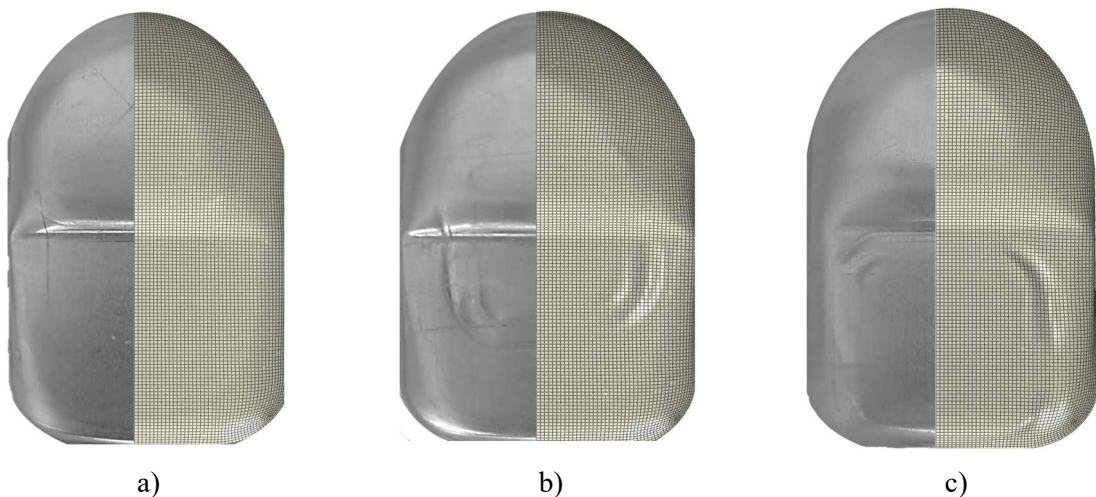
Figure 14 Comparison between the numerical and experimental deformed shapes: a) ID07, b) ID08, c) ID06

3.2.2 Strain path investigation

Once the accuracy of the FE model was assessed, the numerical results were analysed to investigate the nodal strain evolution at different locations. The attention was focused mainly on two groups of nodes: (i) those considered as potentially critical during the reshaping step since being characterized by high level of strain due to the preliminary DD operation (i.e., close to the corner regions) and (ii) those considered as critical during the SHF process (i.e., close to the plane strain condition). Strain path evolutions were thus analysed and, in particular, the ID07 (T_33-57) and the ID06 (B_13-77) were considered, since being characterized by the other two possible locations of the deep drawn feature with respect to the already discussed ID08 (M_33-57).

About ID06 (B_13-77), strain paths concerning the monitored nodes of interest are depicted in Figure 15: continuous lines refer to the strain evolution during the DD step, whereas the dashed lines refer to the strain evolution during the SHF step.
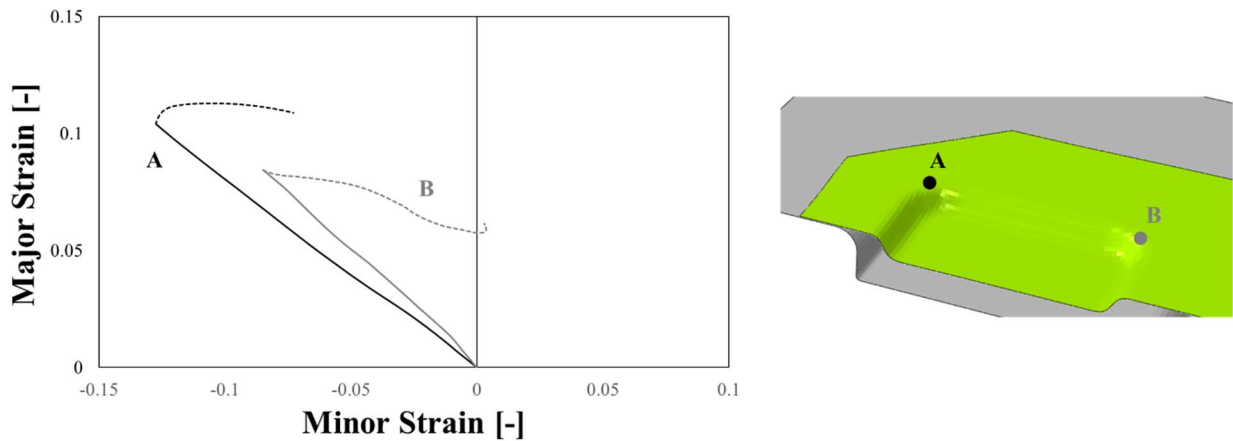

Figure 15 Strain path evolution of relevant nodes (deep-drawing feature located in BOTTOM position, ID06)

Strains of the nodes located in positions A and B (chosen since they experience the contact with the die entry radius during the DD step) were initially characterised by the presence of a negative minor strain (due to the material draw-in). During the SHF step (dashed part of the curve), the major strain remained almost constant, whereas the minor strain moved towards the first quadrant. The analysis suggests that when the existing feature was in the BOTTOM position, the strain experienced by the material during the reshaping step (SHF) was not sufficient to further deform the hardened regions (points A and B) and to convert the existing feature into a new one. In fact, the strain paths of point A and B evolved during the reshaping only in terms of minor strain: the hardened regions were thus not stretched which resulted in a more evident deviation from the reference geometry (as demonstrated in the Figure 8 and Figure 9). The insufficient action to remove the existing feature is probably related also to the low initial value of the BHF which, since promoting the material draw-in, determined an insufficient material stretching. Such a consideration confirms the effectiveness in focussing the attention on the parameter BHF to successfully change the shape of the EoL according to where the existing feature is located. Thus, if the existing feature is located in a position that will be subjected to low strain during the reshaping step, the restraining force exerted by the blankholder needs to be increased.

When the existing feature was located in the TOP position (i.e., ID07 in Figure 16) similar points were considered for the analysis: points A and B showed similar strain evolutions characterized by an almost balanced major and minor strain (slope close to -1) during the DD step.
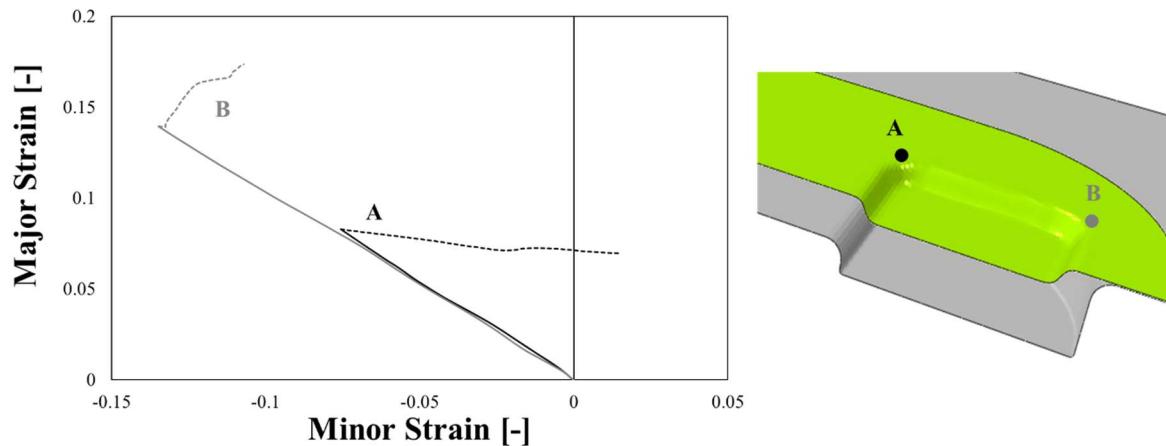

Figure 16 Strain path evolution of relevant nodes (deep-drawing feature located in TOP position, ID 07)

During the reshaping step by SHF, even though the minor strain tended towards the first quadrant in both locations, node B exhibited an increment in the major principal component as a consequence of the die cavity filling. In this case, the strain path of point B changed along the two in-plane directions: as a consequence, the removal of the existing drawn feature was more effective, as also underlined by the lower maximum deviation measured when the existing feature was located in the TOP position. The analysis of the strain path suggested that an effective removal of the existing feature is dependent on its location and on the value of the applied BHF: positioning the feature where higher strains are expected during the reshaping can be more effective for the creation of the new shape.

The sequence of the two manufacturing steps determined deep changes in the strain paths of the monitored nodes, which could be better highlighted by comparing the strain paths of the same node location concerning the two investigated test conditions (ID07 and ID06) with the "Only SHF" condition. For example, Figure 17a shows the comparison concerning the deep drawn feature in the BOTTOM position (ID06): in such a case the position of the feature induced a strain condition more severe than the one occurring in the case the blank was only subjected to SHF. Figure 17b shows that the same occurs in the case the deep drawn feature is located in the TOP position.
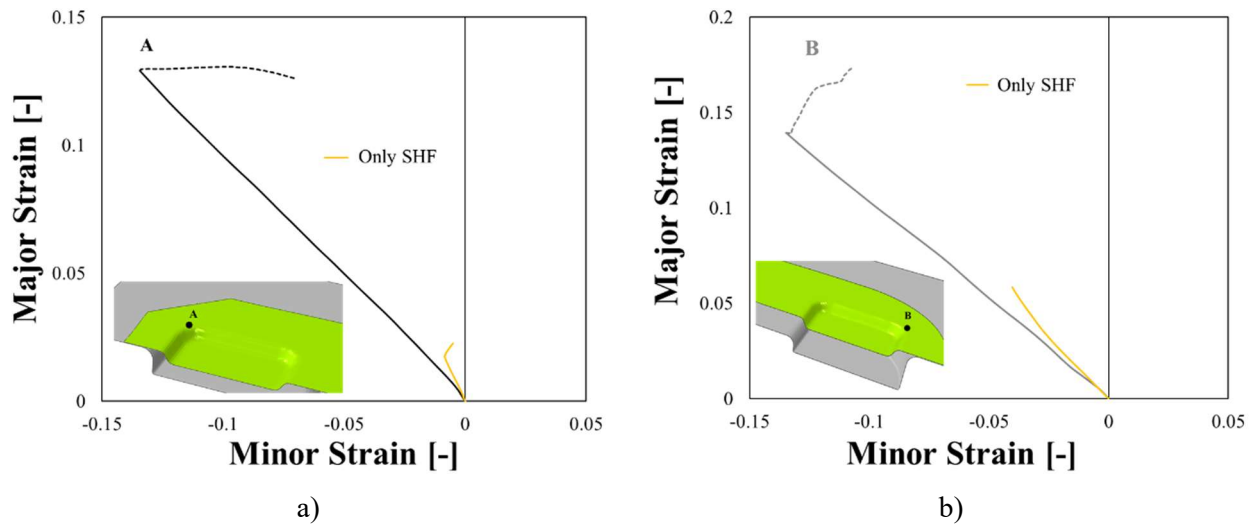
Figure 17 Reshaping vs. SHF: comparison of the strain paths from: a) point A, deep drawn feature in the BOTTOM position (ID06), b) point B, drawn feature in TOP position (ID07)

In the case the SHF is performed using a flat (undeformed) blank the drawing condition imposed by the action of the pressurised oil was less severe than the one reached at the end of the DD, both in terms of path slope and strain level. The analysis of the numerical results was completed by the strain evolution of zones not directly affected by the DD step, but which can be still considered critical for the SHF process. For example, node F (it is in the region where the blank is in contact with the fillet radius between the two depths of the die) shows that in the case of the blank deformed only by SHF (yellow curve in Figure 18), the strain path is close to the plane strain condition. But, in the reshaping process, the preliminary DD step determined a strain condition characterised by a negative minor component (see the green and grey continuous lines) and, once the node came in contact with the die surface (white triangles), it evolved subsequently only in terms of major strain.
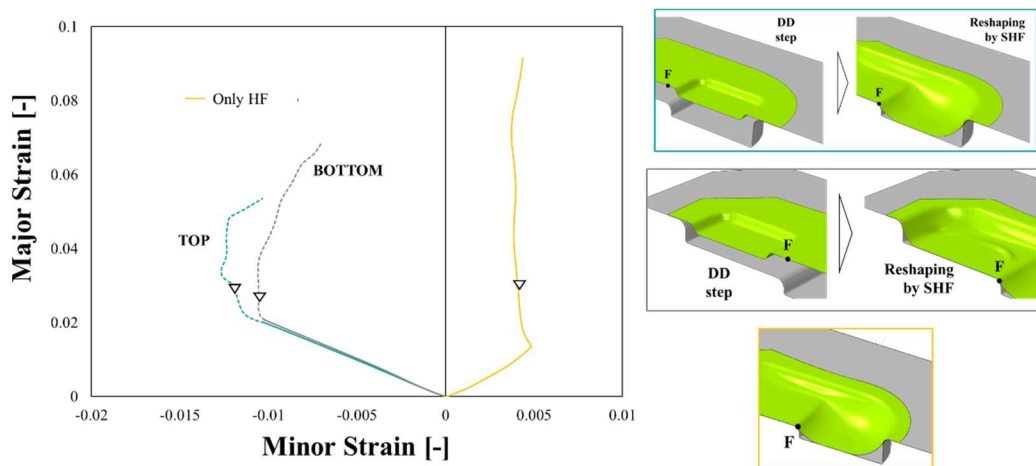

Figure 18 Reshaping (ID07 and ID06) vs. SHF: comparison of the strain paths in the fillet region

3.2.3 Investigation of the blank draw-in

The combination of the two manufacturing steps was analysed in terms of blank draw-in during reshaping by SHF. All outer nodes of the blank were grouped within the same path, and the in-plane displacement was

plotted at the end of the SHF step. Accordingly, the path could ideally be divided into four zones, and the nodal displacements were compared with the reference condition represented by the blank being deformed only by SHF. The comparison in Figure 19 suggests that the material draw-in was restrained in the proximity of the deep drawn feature and, as a consequence, nodes from the Z_1 segment exhibited larger displacements when the drawn feature was located on the opposite side (ID06, drawn feature located in the BOTTOM position).
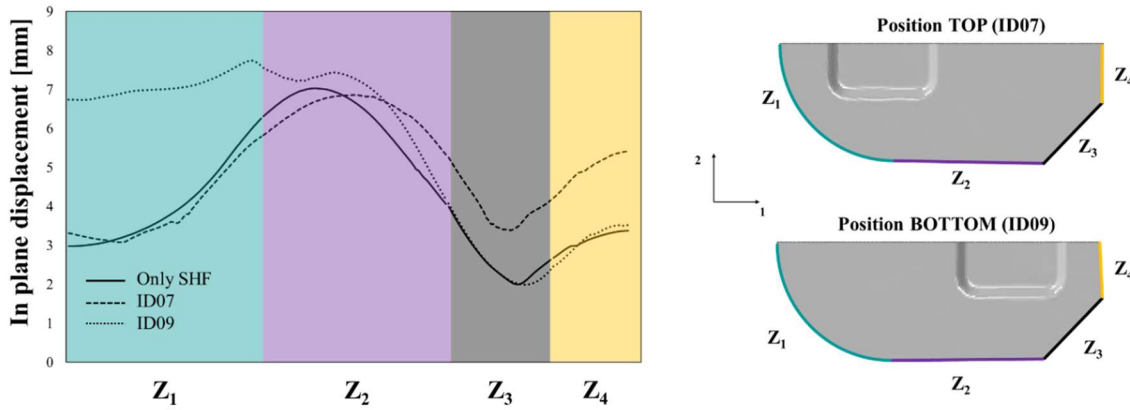

Figure 19 Influence of the deep drawn feature on the blank draw-in during the reshaping by SHF

On the contrary, when the deep drawn feature was located in the TOP position (ID07), the material flow inside the die cavity was more pronounced but less evident than in the other case because of the immediate contact with the shallow step of the die.

Conclusions

In this study, the potentialities of hydroforming as a reshaping process were explored and deeply investigated by means of a numerical model validated using data from a broad experimental campaign.

The selected case study allowed to reproduce a real possible condition in which the shape of an already formed part (end-of-life component) is changed into a new one using the Sheet HydroForming process, thus providing useful data for the validation of the numerical model which was used for investigating the proposed reshaping route. The analysis allowed to point out that the extent of the restraining force, position of the previous feature, and amount of deformation imparted during the reshaping step have an impact on the final results. The following main results can be pointed out:

- the restraining force during the reshaping by SHF (here varied by changing the Blank Holder force) must be sufficiently high to remove the existing feature by enabling stretching mechanics; generally speaking, the higher the level of deformation imparted during the preliminary forming process the higher the restraining force should be; but, since excessively high values of BHF can cause ductile fractures, trade-off values must be identified;

- the presence of a previous geometric feature on the blank affects the SHF process and the output in terms of strain distribution, strain path, geometrical accuracy and quality (in the investigated case study, for example, the previous feature was more visible when located in the bottom region of the two-depth shape);

- as general rule, it can be assumed that the positioning of the EoL component, whose shape has to be changed by SHF, should be decided in order to determine the proper strain level to remove the previous feature, yet taking into account the level and type of strain experienced in the previous forming process. In other words, the feature to be removed should be positioned where higher levels of strain are expected during Reshaping;

- the strain path evolutions of blank regions far from previously deformed zones are poorly affected by the preliminary forming process. Although small differences can be found during the preliminary forming step, the strain path then evolves in the same way it would do if deformed only by the SHF process;

- the strain condition of reshaped components might differ significantly from a conventional hydroformed part, in terms of both strain paths and draw-in displacement. Actually, in-plane displacements of the outer nodes of the flange revealed to be affected by the position of the previous feature: the blank draw-in tends to be remarkably retained close to the blank regions underwent the first forming operation.

Finally, other flexible sheet metal forming processes such as temperature assisted hydroforming and gas forming should be tested for understanding the actual potential of such an approach. The development of these aspects would speed up the industrial applicability of the presented approach.

References

Abu-Farha, F.K., Khraisheh, M.K., 2008. An integrated approach to the Superplastic Forming of lightweight alloys: Towards sustainable manufacturing. Int. J. Sustain. Manuf. 1, 18–40. https://doi.org/10.1504/IJSM.2008.019225

Bell, C., Corney, J., Zuelli, N., Savings, D., 2020. A state of the art review of hydroforming technology. Int. J. Mater. Form. 13, 789–828. https://doi.org/10.1007/s12289-019-01507-1

Brosius, A., Hermes, M., Khalifa, N. Ben, Trompeter, M., Tekkaya, A.E., 2009. Innovation by forming technology: motivation for research. Int. J. Mater. Form. 2, 29–38.

Cao, J., Boyce, M.C., 1997. A Predictive Tool for Delaying Wrinkling and Tearing Failures in Sheet Metal Forming. J. Eng. Mater. Technol. 119, 354–365. https://doi.org/10.1115/1.2812270

Cooper, D.R., Allwood, J.M., 2012. Reusing Steel and Aluminum Components at End of Product Life. Environ. Sci. Technol. 46, 10334–10340. https://doi.org/10.1021/es301093a

Cullen, J.M., Allwood, J.M., 2013. Mapping the Global Flow of Aluminum: From Liquid Aluminum to End-Use Goods. Environ. Sci. Technol. 47, 3057–3064. https://doi.org/10.1021/es304256s

Domitner, J., Silvayeh, Z., Shafiee Sabet, A., Öksüz, K.I., Pelcastre, L., Hardell, J., 2021. Characterization of wear and friction between tool steel and aluminum alloys in sheet forming at room temperature. J. Manuf. Process. 64, 774–784. https://doi.org/10.1016/j.jmapro.2021.02.007

IEA, 2019. Material efficiency in clean energy transitions. https://doi.org/10.1787/aeaaccd8-en

Ingarao, G., Zaheer, O., Campanella, D., Fratini, L., 2020. Re-forming end-of-life components through single point incremental forming. Manuf. Lett. 24, 132–135.

https://doi.org/https://doi.org/10.1016/j.mfglet.2020.05.001

Ingarao, G., Zaheer, O., Fratini, L., 2021. Manufacturing processes as material and energy efficiency strategies enablers: The case of Single Point Incremental Forming to reshape end-of-life metal components. CIRP J. Manuf. Sci. Technol. 32, 145–153. https://doi.org/https://doi.org/10.1016/j.cirpj.2020.12.003

Jeswiet, J., Geiger, M., Engel, U., Kleiner, M., Schikorra, M., Duflou, J., Neugebauer, R., Bariani, P., Bruschi, S., 2008. Metal forming progress since 2000. CIRP J. Manuf. Sci. Technol. 1, 2–17. https://doi.org/10.1016/j.cirpj.2008.06.005

Lang, L.H., Wang, Z.R., Kang, D.C., Yuan, S.J., Zhang, S.H., Danckert, J., Nielsen, K.B., 2004. Hydroforming highlights: sheet hydroforming and tube hydroforming. J. Mater. Process. Technol. 151, 165–177. https://doi.org/10.1016/j.jmatprotec.2004.04.032

Le, V.T., Paris, H., Mandil, G., 2018. The development of a strategy for direct part reuse using additive and subtractive manufacturing technologies. Addit. Manuf. 22, 687–699. https://doi.org/https://doi.org/10.1016/j.addma.2018.06.026

Milovanoff, A., Posen, I.D., MacLean, H.L., 2021. Quantifying environmental impacts of primary aluminum ingot production and consumption: A trade-linked multilevel life cycle assessment. J. Ind. Ecol. 25, 67–78. https://doi.org/https://doi.org/10.1111/jiec.13051

Palumbo, G., Piccininni, A., Guglielmi, P., Di Michele, G., 2015. Warm HydroForming of the heat treatable aluminium alloy AC170PX. J. Manuf. Process. 20. https://doi.org/10.1016/j.jmapro.2015.09.012

Parsa, M.H., Darbandi, P., 2008. Experimental and numerical analyses of sheet hydroforming process for production of an automobile body part. J. Mater. Process. Technol. 198, 381–390. https://doi.org/https://doi.org/10.1016/j.jmatprotec.2007.07.023

Sato, H., Manabe, K., Ito, K., Wei, D., Jiang, Z., 2015. Development of servo-type micro-hydromechanical deep-drawing apparatus and micro deep-drawing experiments of circular cups. J. Mater. Process. Technol. 224, 233–239. https://doi.org/https://doi.org/10.1016/j.jmatprotec.2015.05.014

Sutherland, J.W., Skerlos, S.J., Haapala, K.R., Cooper, D.R., Zhao, F., Huang, A., 2020. Industrial Sustainability: Reviewing the Past and Envisioning the Future. J. Manuf. Sci. Eng. Asme 142.

Takano, H., Kitazawa, K., Goto, T., 2008. Incremental forming of nonuniform sheet metal: Possibility of cold recycling process of sheet metal waste. Int. J. Mach. Tools Manuf. 48, 477–482. https://doi.org/https://doi.org/10.1016/j.ijmachtools.2007.10.009

Tilwankar, A.K., Mahindrakar, A.B., Asolekar, S.R., 2008. Steel recycling resulting from ship dismantling in India: implications for green house gas emissions, in: Proceedings of Second International Conference on "Dismantling of Obsolete Vessels", During. pp. 15–16.

Tolio, T., Bernard, A., Colledani, M., Kara, S., Seliger, G., Duflou, J., Battaia, O., Takata, S., 2017. Design, management and control of demanufacturing and remanufacturing systems. CIRP Ann. 66, 585–609. https://doi.org/https://doi.org/10.1016/j.cirp.2017.05.001

Worrell, E., Allwood, J., Gutowski, T., 2016. The Role of Material Efficiency in Environmental Stewardship. Annu. Rev. Environ. Resour. 41, 575–598. https://doi.org/10.1146/annurev-environ-110615-085737

Zhang, X., Zhang, M., Zhang, H., Jiang, Z., Liu, C., Cai, W., 2020. A review on energy, environment and economic assessment in remanufacturing based on life cycle assessment method. J. Clean. Prod. 255, 120160. https://doi.org/https://doi.org/10.1016/j.jclepro.2020.120160